INTERNATIONAL JOURNAL OF RESEARCH AND TECHNOPRENEURIAL INNOVATIONS (IJRTI)

Volume 1 Issue 1 (April 2024)

Central Instrument Laboratory, University of Port Harcourt, Nigeria
E-mail: centralinstumentlaboratory@uniport.edu.ng

Computational Study of the Structural, Electronic and Optical Properties of Cubic Phase Y_2MgX_4 (X = S, Se and Te) Metal Chalcogenide Compounds

Abdu Barde[1, *], Alhassan Umar Haruna[2]

[1] Department of Science laboratory Technology, Jigawa State Polytechnic, Dutse, Nigeria
2 Department of Computer Science, Jigawa State Polytechnic, Dutse, Nigeria

Email address:

[*]Corresponding author: abdubarde@jigpoly.edu.ng

To cite this article: Barde, A. and Haruna, A.U. Computational Study of the Structural, Electronic and Optical Properties of Cubic Phase Y_2MgX_4 (X = S, Se and Te) Metal Chalcogenide Compounds. *International Journal of Research and Technopreneurial Innovations* 2024; 1(1): 129-138.

Keywords:
Y_2MgX_4,
Metal-chalcogenides,
DFT,
Approximations

ABSTRACT

In this work, first principles density functional theory (DFT) was employed to gain computational insight into ground state, electronics and optical properties of Y_2MgX_4(X = S, Se, and Te) metal chalcogenides. The result of ground state properties reveals that Y_2MgX_4 compounds are mechanically and dynamically stable against mechanical distortions. Electronic properties determined using the generalized gradient approximation (GGA) and Tran-Blaha (meta-GGA) functional, shows that Y_2MgX_4 compounds are semiconductor materials. The chalcogenides atoms considerably engineered the band gap from Sulphur to Tellurium atoms. For the optical properties, Greens function (GW) was employed for the calculation of optical band gap. The Bether-Salpeter equation (BSE) applied together with GW to compute the frequency-dependent dielectric function and absorption coefficient. The estimated optical band gap from the BSE calculations are 2.35 eV, 2.02 eV and 1.12 eV and that of the meta-GGA are 2.65 eV, 2.15 eV and 1.19 eV for Y_2MgS_4, Y_2MgSe_4, and Y_2MgTe_4 metal chalcogenides respectively. The results from the two calculation are comparable. Both calculations suggest that Y_2MgX_4 compounds are semiconductor materials and are suitable candidates for energy conversion applications.

1. INTRODUCTION

Metal chalcogenides have received significant attention in the past decades, compounds in binary A_2Q(A = K, Rb, Cs; Q= Se, Te) [1], ternary $Ba_4Ga_2Se_8$[2] and quaternary $KBiMS_4$(M= Si, Ge) [3], $Ba_5Al_2Se_8$ and $Ba_5Ga_2Se_8$ [4] phases have been studied both theoretically and experimentally. The physical properties, structural diversity and the importance of the metal chalcogenides have been reported [5]. Part of its potential technological importance and applications reported are in the area of thermoelectric heat energy conversion [6 - 7], photocatalytic and photovoltaic [8] solar energy conversion, and light emitting devices [9]. These applications highlighted the importance of metal chalcogenides in solving potential problems concerning environmental pollution and energy crises.

Computational techniques using the state-of-art, the first-principle calculation have been very successful in predicting the ground state, stability, electronic and optical properties of a metal

chalcogenides compounds [10-11,13–15]. In density functional theory calculations, the ground state properties such as structural properties, elastic and dynamical stabilities are computed from well-known established procedures, the Born stability criteria [16] and finite displacement techniques [17]. These techniques provide reliable data on material response to external forces and perturbation, they predicted Young, bulk and shear modulus, Poison ratio and elastic constant [18] and also the phonon dispersion accurately.

Similarly, the first-principle method using the well-known functional the generalized gradient approximation (GGA-approximation) and Meta-GGA are used to study electronic and optical properties. The Green's function (GW) method is found to predict the electronic and optical properties close to experimental values. The growing interest in the search for a sustainable and renewable alternative energy materials for energy conversion in the area of photovoltaic, photochemical cells, photo-catalyst and thermoelectric heat energy conversion [18–20], the renewable global status report 2019 (GSR2019) [21] highlighted that by 2040 the source of renewable energy is expected to increase by 45% from solar, wind and hydrothermal. In line with above prediction the discoveries of metal chalcogenides [3,5-6,22] were known to contribute significantly in the drive to sustainable renewable energy. According to the studies conducted on metal chalcogenides [18-20] suggested that metal chalcogenides semiconductors materials with suitable band gap of 1.3 eV and > 1.8 eV can be useful for photovoltaic and photocatalytic materials. This prediction is also in conformity with report from [8,23] that materials with band gap 1.3 eV and > 1.8 eV are potential candidate for solar cell and photocatalytic materials.

The role of metal chalcogenides as energy conversion materials motivate our study of Y_2MgX_4(X= S, Se, Te) metal chalcogenides compound. In the study, we use the first principle technique to establish the ground state structure, mechanical and dynamical stabilities, and the electronic and optical properties of Y_2MgX_4 metal chalcogenides compound. Calculations using the density functional theory with the generalized gradient approximation (DFT-GGA) [24] provide reliable calculations of structural parameters, and mechanical and dynamical properties of crystals. We believed this work will open further research opportunities in the area of applications of Y_2MgX_4 metal chalcogenides.

2. MATERIALS AND METHODS

2.1. Computational details

In this study, we investigate the equilibrium structural parameters mechanical and dynamic stabilities of Y_2MgX_4 metal chalcogenides using the density functional theory (DFT) [25-26] as implemented in the Vienna ab initio simulation package (VASP) [27-28]. VASP is a plane-wave all-electron code that implements a plane-wave basis set using projected-augmented-wave (PAW) [29] formulation for the description of electron-ion interactions. In solving the self-consistent Kohn-Sham (KS) Schrödinger like Eigen equation given by [25]:

$$\left\{\frac{-\hbar^2}{2M_e}\nabla_i^2 + \int\frac{n(r')}{|r-r'|} + V_{ext}(r) + V_{XC}^{\sigma,k}[n(r)]\right\} \psi_i^{\sigma,k}(r)\epsilon_i^{\sigma,k}\psi_i^{\sigma,k}(r) \quad (1)$$

VASP expands the Pseudo part of Kohn-Sham one-electron spin orbitals $\psi_i^{\sigma,k}(r)$ on a basis set of plane-waves. Groundstate energies were calculated within the Perdew-Burke-Ernzehof generalized gradient approximation as revised for solids and their surfaces, PBEsol [24], for the electron exchange-correlation energy. Equilibrium structure optimization was conducted on the primitive cell structure. We include the plane-wave with kinetic energy $\frac{-\hbar^2}{2M_e}|K-G| < E_{cut}$. For this investigated system energy cut-off E_{cut} is set to 520 eV and the kpoints sampling of 4 x 4 x 4 Monkhorst-pack mesh [30] is used for sampling the Brillouin zone. The k-point mesh sampling was

chosen to achieve convergence energies within less than 1.0 meV/atom. The elastic tensor was calculated from the fully relaxed equilibrium geometry with PBEsol [24]. A supercell method was employed with 2 x 2 x 2 supercells of the unit cell, to calculate phonon dispersion curves with a finite displacement method as implemented in the PHONOPY package [31] to study the dynamic properties. Electronic band structures are calculated using the generalized gradient approximation PBEsol functional and modified Becker Johnson potential (MBJ) [32]. The MBJ-GGA potential (V_{XC}) uses the mBJ exchange potential together with the GGA correlation potential to performs the calculation of band gaps which reproduce band gap similar to the GW calculations. The mBJ exchange potential (V_{XC}) is defined as:

$$V_{x,\sigma}^{MBJ}(r) = cv_{x,\sigma}^{B,R}(r) + (3c - 2)\frac{1}{\pi}\sqrt{\frac{5}{12}}\sqrt{\frac{2t_\sigma(r)}{\rho^\sigma(r)}} \quad (2)$$

where $\rho^\sigma = \sum_{j=1}^{N_\sigma}|\psi_{i,\sigma}|^2$ is the electronic density, t_σ is kinetic energy density and $v_{x,\sigma}^{BR}$ is the Becke-Roussel (BR) [33] potential which was proposed to model the Coulomb potential created by the exchange hole. c in the Equation is chosen to be linearly dependent on the square root of the average of $\frac{|\nabla|}{\rho}$.

Moreover, in this study we performed a post-DFT, the so called many-body Green's function G_0W_0 [34 - 36], to obtained the estimate of the quasi-particle excitation. We used a 180 eV energy cut-off for the response functions to determine the fundamental gaps. Finally, the optical absorption spectrum was obtained by including excitonic effects using the G_0W_0 together with Bethe-Salpeter Equation (BSE) [34 - 35], [37] approximation. From the optical absorption spectra, the positions of the optical band gap were determined using Tauc plots [38].

3. RESULTS AND DISCUSSION

3.1 Structural properties

The structure of a primitive unit cell and Brillioun zone of Y_2MgX_4 are shown in Figure 1 and Figure 2 respectively. From the optimized structure of Y_2MgX_4, we derived the ground state properties. The energy of cohesion, optimized volume, bulk modulus, and its pressure derivatives are determined by fitting the total energy to the well-known 3rd order Murnaghan's equation of state (EOS) (3) [39], the least-square method. The method is widely used to extract the equilibrium parameters from (3). The energy-volume relationship is displayed in Figure 3, 4 and 5.

$$E(V) = E_0 + \frac{9B_0V_0}{16}\left\{\left[\left(\frac{V_0}{V}\right)^{\frac{2}{3}} - 1\right]^3 B_0'\right\} + \left[\left(\frac{V_0}{V}\right)^{\frac{2}{3}} - 1\right]^2\left[6 - 4\left(\frac{V_0}{V}\right)^{\frac{2}{3}}\right] \quad (3)$$

where E_0 V_0, B_0 and B_0' are equilibrium cohesive energy, equilibrium volume, the bulk modulus, and its pressure derivatives.

where E_0 V_0, B_0 and B_0' are equilibrium cohesive energy, equilibrium volume, the bulk modulus, and its pressure derivatives.

The energy of cohesive (E_{coh}) is the energy required to decompose a solid into its constituents. The more negative energy, the more energetically favorable and stable the constituent atoms mixed to form a stable compound [40]. The structural parameters, E_0 V_0, B_0, B_0' and E_{coh} are equally mention in Table 1 and 2.

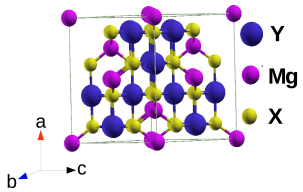

Figure 1. Craystal structure of Y_2 MgX_4 .

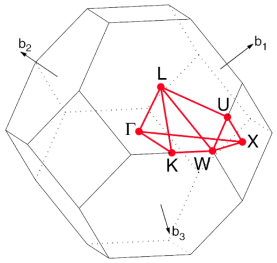

Figure 2. First Brillious zone of Y_2MgX_4 unit cells.

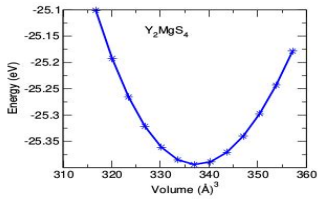

Figure 3. Variation of total energy as a function of volume for Y_2MgS_4..

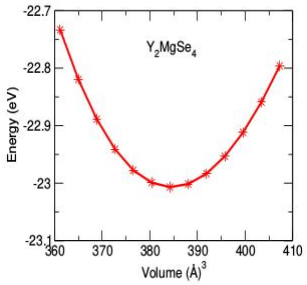

Figure 4. Variation of total energy as a function of volume for Y_2MgSe_4.

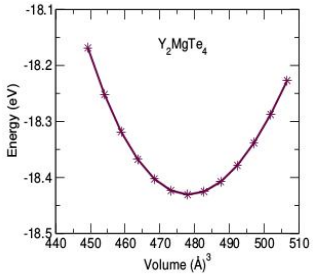

Figure 5. Variation of total energy as a function of volume for Y_2MgTe_4..

Table 1. Calculated lattice parameters a, b, c (Å), volumes in Angstrom, angles α, β, γ in degrees.

Compounds	a=b=c	Volume (V)	α, β and γ
Y_2MgS_4	7.90	348.54	90
Y_2MgSe_4	8.16	384.50	90
Y_2MgTe_4	8.78	478.24	90

Table 2. bulk modulus B_0 in Giga Pascal (GPa), derivative of Bulk Modulus B_0' and cohesive energy E_{coh} in eV.

Compounds	B_0	B_0'	E_{coh}
Y_2MgS_4	61.97	4.25	-5.06
Y_2MgSe_4	51.58	3.92	-4.98
Y_2MgTe_4	42.86	4.38	-4.41

3.2 Elastic stabilities

We calculated the elastic constant to investigate the mechanical stability of Y_2MgX_4. Y_2MgX_4 is a cubic structure in Fd-3̄m symmetry (space group 227) and has three independent elastic constants C_{11}, C_{12} and C_{44}. We compute the elasticity components of C_{ij} using the energy – strain relationship method described by [41]. The elastic constant is calculated using PBEsol functional and the values are depicted in Table 2. Also, depicted are the calculated bulk modulus (B_H), shear modulus (G) and Young modulus (E) all in GPa and the Poissons ratio calculated using the Hill approach [42]. To the best of our knowledge there is no theoretical or experimental values to use for comparison. To ensure the reliability of our calculation, the calculated elastic constant is checked by well-known Born-stability criteria [41] for cubic crystals [43]. Born-stability criteria are a set of elastic constant (C_{ij}) conditions that are related to the second-order change in the internal energy of a crystal under deformation. These criteria can be derived by applying the convexity condition on (4).

$$C_{11} - C_{12} > 0, C_{11} + 2C_{12} > 0, C_{44} > 0 \quad (4)$$

The listed elastic constants in Table 3, satisfy all Born stability criteria for the mechanical stability stated in (4) for the cubic crystal. From the reliability conditions, Y_2MgX_4 are mechanically stable compounds. The values of the Poisson's ratio listed in Table 4 0.35, 0.38, 0.38 for Y_2MgS_4, Y_2MgSe_4 and Y_2MgTe_4 respectively reveals that all the compound possess ionic bonding. Since the Poisson's ratio (ν) determined are greater than 0.25. To investigate material response to external forces the Bulk and shear moduli are calculated, the chalcogenides atoms in the material structure of Y_2MgX_4 brings a considerable decrease in bulk moduli as well as the shear modulus. This indicates that there are increase in compressibility and decrease in resistance to plastic deformations from S to Te chalcogenide atoms of Y_2MgX_4 this is seen in Table 4.

Table 3. Calculated values of independent elastic constant C_{11}, C_{12} and C_{44} Giga Pascal (GPa).

Compound	C_{11}	C_{12}	C_{44}
Y_2MgS_4	84.38	57.04	29.86
Y_2MgSe_4	66. 36	32.56	23.75
Y_2MgTe_4	47.32	37.01	16.96

Table 4. The Bulk modulus B_H, the Young Modulus E and Shear Modulus G all in (GPa) and the Poisson's ratio *v*.

Compound	B_H	E	G	*v*
Y_2MgS_4	66.15	58.98	21.82	0.35
Y_2MgSe_4	57.16	40.15	14.51	0.38
Y_2MgTe_4	40.45	29.10	10.54	0.38

3.3 Dynamical stabilities

Phonon band structure, the total and projected density of states (TPDOS) of Y_2MgX_4 computed with PBEsol are shown in Figure [6 - 7] and 8 respectively. In harmonic approximation the dynamic properties of a compound are obtained by solving the eigenvalue problem of the dynamical matrix D(q) [44 - 45]

$$\sum_{\beta k'} D_{kk'}^{\alpha\beta}(q)\epsilon_{qj}^{\beta k'} = \omega_{qj}^2 \epsilon_{qj}^{\alpha k} \quad (5)$$

and the atomic contribution to DOS of phonon density of state is given by the relation:

$$g(\omega) = \frac{1}{N}\sum_{qj} \delta\left(\omega - \omega_{qj}\right) \quad (6)$$

In (5) D(q) is the dynamical matrix, ϵ_{qj} and ω_{qj} are the phonon polarization and frequency respectively. While in (6) N is the number of unit cells in Born-Von Karman supercell and is determined by the choice of kpoints and g(ω) is the density of state. Calculated phonon dispersion mode display along the high-symmetry kpaths shown in Figure 6, 7 and 8 have no negative frequencies, which indicates that Y_2MgX_4 structures are dynamically stable. There are 14 atoms in a unit cell of Y_2MgX_4 structures, and 42 independent vibration modes can be found, from the 42, there are 3 acoustic mode and the remaining are optical mode. Careful examination of PDOS reveals that in Figure 6 the acoustic modes are dominated by the Y atom and the optical modes by the S atom. In Figure 7 both the acoustic and optical modes are dominated by the Se atom, while in Figure 8 Te atom dominating the acoustic mode with Y atom dominating the optical mode of vibration.

3.4 Electronic properties

Electronic band structure calculations were studied with PBEsol (GGA) [24] and MBJ functional (Meta-GGA) [32] with basic generalized Kohn-Sham method [20] which approximates the derivative discontinuity of the exact exchange potential for the band structure calculation. The combined band structure, total density of state (TDOS), and projected density of state (PDOS) are displayed in Figure 9, 10 and 11 for comparison. The PBEsol approximation is reported always to underestimate the band gap [46].

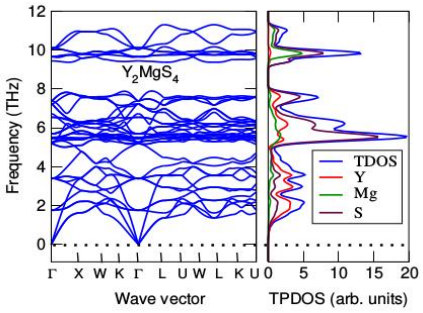

Figure 6. Phonon dispersion with TDOS and PDOS for Y_2MgS_4.

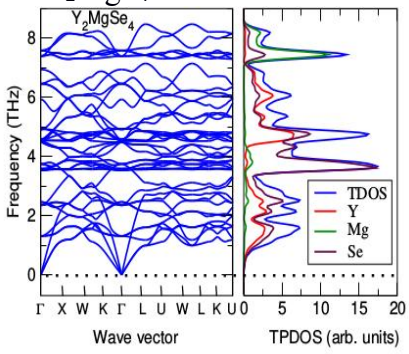

Figure 7. Phonon dispersion with TDOS and PDOS for Y_2MgSe_4.

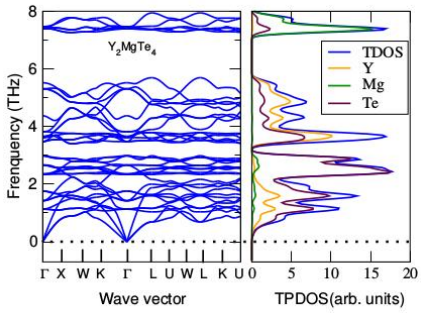

Figure 8. Phonon dispersion with TDOS and PDOS for Y_2MgTe_4.

To improve the representation of the band structures, we employed the meta-GGA that is reported on average to reproduces band gaps with about 10% error compared to experiment and GW calculation [30]. Figure 9, 10 and 11 are band structures determined from the high symmetry kpaths direction in the Brillouin zone. In Figure 9, 10 and 11, we show that Y_2MgX_4 compounds are direct band gap materials. Also, shown are the locations of GGA and meta-GGA band gap GGA(red) and metaGGA(blue). The GGA under estimated the band gaps of Y_2MgX4 and the meta-GGA improves the band gaps by causing the rigid displacement of the conduction band toward higher energy. It is well-known that Energy band gaps calculated with Meta-GGA are comparable to the GW calculations. Hence, for an accurate description of band gap energies, we employed Green's function G_0W_0 approach. For comparison, the computed band gap base on GGA, Meta-GGA, and G_0W_0 (fundamental gap) and the G_0W_0 together with BSE (optical gap) are listed in Table 5.

In Figure 9. 10 and 11, the right side of each band-structure is the calculated total density TDOS, which is the sum of atomic contribution of Y_2MgX_4 compounds. The projected density of state PDOS which is the contribution of the individual atom, with Fermi-level set at zero. It is observed from PDOS that the lower conduction bands are dominated by the contribution of Y-(4d) and the upper valence bands are dominated by the contribution of chalcogenides atoms (X= S, Se, and Te-(4p) respectively.

Our calculation revealed the impacts and effects of the chalcogenide S, Se, and Te atoms composition on electronic properties of Y_2MgX_4 compounds. The substitutions of chalcogenide atoms in Y_2MgX_4 engineered the band gaps. There is a decreasing in band gap value from S atom to Te atom. This characteristic is important in determining the applications of the semiconductor materials.

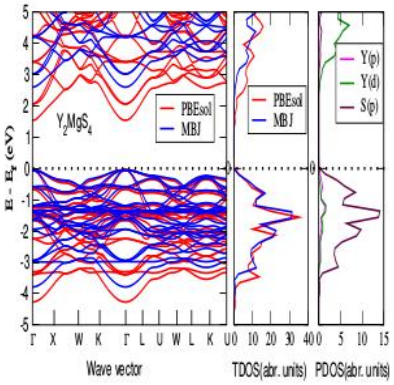

Figure 9. Electronic band structures calculated using PBEsol (red) and MBJ (blue), total (TDOS) and projected (PDOS) density of state compared along high symmetry points for Y_2MgS_4.

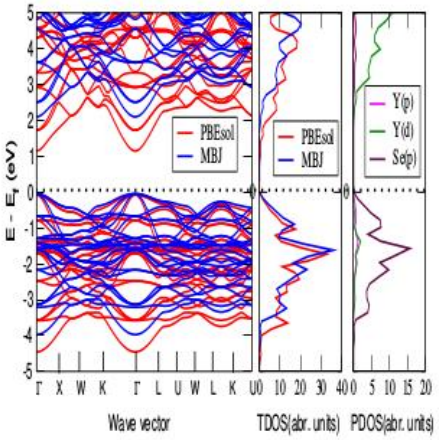

Figure 10. Electronic band structures calculated using PBEsol (red) and MBJ (blue), total (TDOS) and projected (PDOS) density of state compared along high symmetry points for Y_2MgSe_4.

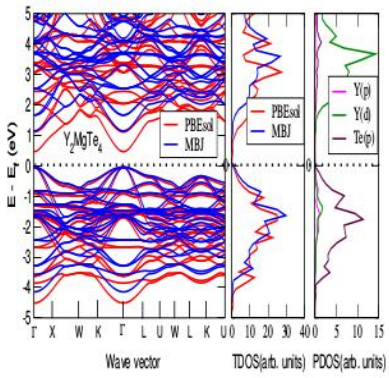

Figure 11. Electronic band structures calculated using PBEsol (red) and MBJ (blue), total (TDOS) and projected (PDOS) density of state compared along high symmetry points for Y_2MgT_4.

Table 5. Calculated band gap in (eV) from PBEsol, MBJ, functionals, and G_0W_0, BSE approximations.

Compound	PBEsol	MBJ	G_0W_0	BSE
Y_2MgS_4	1.58	2.65	3.06	2.35
Y_2MgSe_4	1.21	2.15	2.51	2.02
Y_2MgTe_4	0.51	1.19	1.47	1.12

3.5 Optical properties

Optical properties are directly related to electronic properties, it described the materials optical gaps from the dielectric function for a better understanding of material applications. The complex dielectric function $\varepsilon(\omega) = \varepsilon_1(\omega) + \varepsilon_2(\omega)$ provides information about optical properties of materials, the polarization response to an external applied electric field and photon absorption. The imaginary part $\varepsilon_2(\omega)$ of the complex dielectric function is expressed as the momentum matrix elements between the occupied and unoccupied electronic states as defined by (7) [47]:

$$\varepsilon_2(\omega) = \frac{2e^2\Pi}{\Omega\epsilon_0}\left|\left\langle \psi_k^c \left| \hat{u}.\vec{r} \right| \psi_k^v \right\rangle\right|^2 \delta\left(E_k^c - E_k^v - E\right) \quad (7)$$

where ω is the light frequency, ϵ is the electronic charge, û is the vector defining the polarization of the incident electric field, and ψ_k^c, ψ_k^v are the conduction and valence band wave functions at k respectively.

The real part ε_1 is derived from the imaginary part by a Kramers-Kronig transformation relations [48]. Other optical parameters such as the refractive index n(ω), extinction coefficient k(ω), optical reflectively R(ω), absorption coefficient α(ω), and energy loss functions L(ω) can be calculated from the complex dielectric function ε(ω) [49]. The imaginary part of the dielectric function ε_2 (ω) is a quantity that explains the actual response in the band structure plot in relation to the absorption behavior of a material.

Figure 12, 13 and 14 shows the optical absorption spectra which is determined from the imaginary functions $\varepsilon_2(\omega)$ of the complex dielectric. The positions of the optical gap on the absorption spectra Figure 12, 13 and 14 are determined using the Tauc method [38]. On the absorption spectra, the method determines the absorption edge by linearly extrapolating $(\alpha h\upsilon)^{\frac{1}{n}}$ to zero x-axis using equation $\alpha h\upsilon = K\left(h\upsilon - E_g\right)^n$, where K is proportionality constant, hν is the photon energy, Eġ is the energy gap and n the exponential with values represented by 2, $\frac{1}{2}$, $\frac{2}{3}$ and $\frac{1}{3}$ for direct, indirect, allowed and forbidden transitions respectively. The absorption edge according to the Tauc plots seen in Figure 12, 13 and 14 are located at 2.35, 2.02, and 1.12 eV for Y_2MgS_4, Y_2MgSe_4, and Y_2MgTe_4 respectively, and from our band structure calculations both are direct transition. This confirmed our band-structure calculation, and the energy gaps listed in Table 5. From the Tauc absorption values, it is observed that Y_2MgS_4, Y_2MgSe_4 and Y_2MgTe_4 compounds have good optical absorption in both the visible and infrared regions.

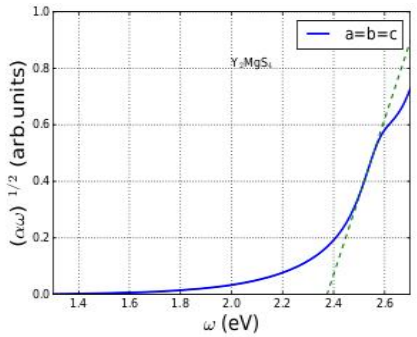

Figure 12. Tauc plot from the BSE absorption spectra fitting the linear region to evaluate the band gap at x-intercepts for Y_2MgS_4.

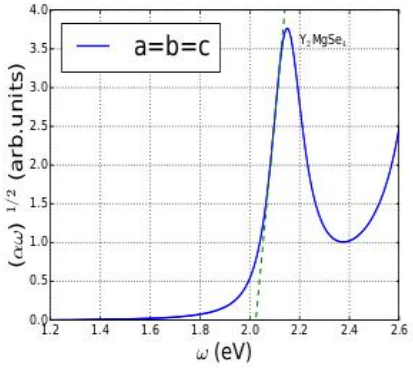

Figure 13. Tauc plot from the BSE absorption spectra fitting the linear region to evaluate the band gap at x-intercepts for Y_2MgSe_4.

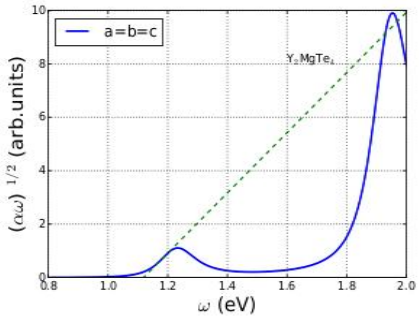

Figure 14. Tauc plot from the BSE absorption spectra fitting the linear region to evaluate the band gap at x-intercepts for Y_2MgTe_4.

4. CONCLUSIONS

We successfully use the density functional theory to study the structural, electronic, and optical properties of metal chalcogenides Y_2MgX_4(X= S, Se, and Te). The calculated structural parameters including the energy-volume equation of state (EOS), equilibrium lattice structural parameters, and the cohesive energy reveals that Y_2MgX_4 are cubic phase structures. The calculated independent elastic constant, bulk modulus, shear modulus, Young modulus, cohesive energy, and Poisson's ratio shows that the compounds are mechanically stable and can be synthesized. Phonon calculations of Y_2MgX_4 compounds indicate they are dynamically stable, negative vibrations are not seen in Figure 6, 7 and 8. The electronic structure and optical property calculations reveal that Y_2MgX_4 compounds can absorb light in the visible and infrared regions. These properties are calculated for the first time and we hope that the present work will serve as a reference for other theoretical and experimental studies on the metal chalcogenides Y_2MgX_4 compounds and their potential applications.

5. Acknowledgements.
We acknowledge the Centre for High-Performance Computing (CHPC), South Africa, for providing computational resources to this work.

References

[1] Chakraborty, G., Park, I. H., Medishetty, R. and Vittal, J. J. (2021). Two-dimensional metal-organic framework materials: synthesis, structures, properties and applications. *Chemical Reviews, **121**, 3751-3891.*

[2] Yin, W., Iyer, A. K., Lin, X. and Mar, A. (2016). Ba4Ga2Se8: A ternary selenide containing chains and discrete Se22− units. *Journal of Solid State Chemistry, **237**, 144-149.*

[3] Mei, D., Lin, Z., Bai, L., Yao, J., Fu, P. and Wu, Y. (2010). KBiMS4 (M= Si, Ge): Synthesis, structure, and electronic structure. *Journal of Solid State Chemistry, **183**, 1640-1644.*

[4] Mei, D., Yin, W., Lin, Z., He, R., Yao, J., Fu, P. and Wu, Y. (2011). Syntheses and characterization of two new selenides Ba5Al2Se8 and Ba5Ga2Se8. *Journal of alloys and compounds, **509**, 2981-2985.*

[5] Gauthier, G., Kawasaki, S., Jobic, S., Macaudière, P., Brec, R. and Rouxel, J. (1998). Characterization of Ce 3 (SiS 4) 2 I, a compound with a new structure type.

*Journal of Materials Chemistry, **8**, 179-186.*

[6] Mahmoud, M. M., Joubert, D. P. and Molepo, M. P. (2019). Structural, stability and thermoelectric properties for the monoclinic phase of NaSbS 2 and NaSbSe 2: A theoretical investigation. *The European Physical Journal B, **92**, 1-15.*

[7] Abdulsalam, M., Rugut, E. and Joubert, D. P. (2020). Mechanical, thermal and thermoelectric properties of MX2 (M= Zr, Hf; X= S, Se). *Materials Today Communications, **25**, 101434.*

[8] Chen, M. M., Xue, H. G. znd Guo, S. P. (2018). Multinary metal chalcogenides with tetrahedral structures for second-order nonlinear optical, photocatalytic, and photovoltaic applications. *Coordination Chemistry Reviews, **368**, 115-133.*

[9] Drief, F., Tadjer, A., Mesri, D. and Aourag, H. (2004). First principles study of structural, electronic, elastic and optical properties of MgS, MgSe and MgTe. *Catalysis Today, **89**, 343-355.*

[10] Pandey, R. and Sutjianto, A. (1994). Study of structural phase transition in MgSe. *Solid state communications, **91**, 269-271.*

[11] Waag, A., Fischer, F., Lugauer, H. J., Litz, T., Laubender, J., Lunz, U. and Landwehr, G. (1996). Molecular-beam epitaxy of beryllium-chalcogenide-based thin films and quantum-well structures. *Journal of Applied Physics, **80**, 792-796.*

[12] Tairi, L., Touam, S., Boumaza, A., Boukhtouta, M., Meradji, H., Ghemid, S. and Khenata, R. (2017). Phase stability and electronic behavior of MgS, MgSe and MgTe compounds. *Phase Transitions, **90**, 929-941.*

[13] Xiao-Cui, Y., Ai-Min, H., Jie, Y., Yong-Hao, H., Gang, P., Chun-Xiao, G. and Guang-Tian, Z. (2008). Theoretical prediction for structural stabilities and optical properties of SrS, SrSe and SrTe under high pressure. *Chinese Physics Letters, **25**, 1807.*

[14] Ren, Y. (2017). First principles study of electronic, phonon and elastic properties of rock-salt-phase MTe (M= Mg, Ca, Sr, Ba). *Computational Condensed Matter, **11**, 69-76.*

[15] Bouhemadou, A., Khenata, R., Zegrar, F., Sahnoun, M., Baltache, H. and Reshak, A. H. (2006). Ab initio study of structural, electronic, elastic and high pressure properties of barium chalcogenides. *Computational Materials Science, **38**, 263-270.*

[16] Born, M. and Fürth, R. (1940). The stability of crystal lattices. III: an attempt to calculate the tensile strength of a cubic lattice by purely static considerations. In *Mathematical Proceedings of the Cambridge Philosophical Society, Cambridge, 4 October 1940, 454-465.*

[17] Yuan, P. F. and Ding, Z. J. (2008). Ab initio calculation of elastic properties of rock-salt and zinc-blend MgS under pressure. *Physica B: Condensed Matter, **403**, 1996-1999.*

[18] Luo, B., Ye, D. and Wang, L. (2017). Recent progress on integrated energy conversion and storage systems. *Advanced Science, **4**, 1700104.*

[19] Green, M. A. and Bremner, S. P. (2017). Energy conversion approaches and materials for high-efficiency photovoltaics. *Nature materials, **16**, 23-34.*

[20] Li, C., Cao, Q., Wang, F., Xiao, Y., Li, Y., Delaunay, J. J. and Zhu, H. (2018). Engineering graphene and TMDs based van der Waals heterostructures for photovoltaic and photoelectrochemical solar energy

conversion. *Chemical Society Reviews, **47**, 4981-5037.*

[21] Raturi, A. K. (2019). Renewables 2019 global status report.

[22] Shockley, W. and Queisser, H. (2018). Detailed balance limit of efficiency of p–n junction solar cells. In *Renewable Energy 35 - 54.*

[23] Khaselev, O. & Turner, J. A. (1998). A monolithic photovoltaic-photoelectrochemical device for hydrogen production via water splitting. *Science, **280**, 425-427.*

[24] Perdew, J. P., Ruzsinszky, A., Csonka, G. I., Vydrov, O. A., Scuseria, G. E., Constantin, L. A. and Burke, K. (2008). Restoring the density-gradient expansion for exchange in solids and surfaces. *Physical review letters, **100**, 136406.*

[25] Kohn, W., & Sham, L. J. (1965). Self-consistent equations including exchange and correlation effects. *Physical review, **140**, A1133.*

[26] Hohenberg, P. and Kohn, W. (1964). Inhomogeneous electron gas. Physical review, **136**, B864.

[27] Kresse, G. and Furthmüller, J. (1996). Efficient iterative schemes for ab initio total-energy calculations using a plane-wave basis set. *Physical review B, **54**, 11169.*

[28] Kresse, G. and Furthmüller, J. (1996). Efficiency of ab-initio total energy calculations for metals and semiconductors using a plane-wave basis set. *Computational materials science, **6**, 15-50.*

[29] Kresse, G. and Joubert, D. (1999). From ultrasoft pseudopotentials to the projector augmented-wave method. *Physical review b, **59**, 1758.*

[30] Monkhorst, H. J. and Pack, J. D. (1976). Special points for Brillouin-zone integrations. *Physical review B, **13**, 5188.*

[31] Togo, A. (2009). Phonopy http://phonopy. sourceforge. Net.

[32] Tran, F. and Blaha, P. (2009). Accurate band gaps of semiconductors and insulators with a semilocal exchange-correlation potential. P*hysical review letters, **102**, 226401.*

[33] Becke, A. D. and Roussel, M. R. (1989). Exchange holes in inhomogeneous systems: A coordinate-space model. *Physical Review A, **39**, 3761.*

[34] Hanke, W. and Sham, L. J. (1980). Many-particle effects in the optical spectrum of a semiconductor. *Physical Review B, **21**, 4656.*

[35] Onida, G., Reining, L. and Rubio, A. (2002). Electronic excitations: density-functional versus many-body Green's-function approaches. *Reviews of modern physics, **74**, 601.*

[36] Hedin, L. and Lundqvist, S. (1970). Effects of electron-electron and electron-phonon interactions on the one-electron states of solids. *In Solid state physics **23**, 1-181.*

[37] Salpeter, E. E. and Bethe, H. A. (1951). A relativistic equation for bound-state problems. *Physical Review, **84**, 1232.*

[38] Tauc, J., Grigorovici, R. and Vancu, A. (1966). Optical properties and electronic structure of amorphous germanium. *physica status solidi (b), **15**, 627-637.*

[39] Murnaghan, F. D. (1944). The compressibility of media under extreme pressures. Proceedings of the National *Academy of Sciences, **30**, 244-247.*

[40] Hosseini, S. M., Movlarooy, T. and Kompany, A. (2007). First-principle calculations of the

cohesive energy and the electronic properties of PbTiO3. *Physica B: Condensed Matter, **391**, 316-321.*

[41] Born, M. (1954). K. Huang Dynamical theory of crystal lattices. *Oxford University Press.*

[42] Hill, R. (1963). Elastic properties of reinforced solids: some theoretical principles. *Journal of the Mechanics and Physics of Solids, **11**, 357-372.*

[43] Karki, B. B., Ackland, G. J. and Crain, J. (1997). Elastic instabilities in crystals from ab initio stress-strain relations. *Journal of Physics: Condensed Matter, **9**, 8579.*

[44] Togo, A., & Tanaka, I. (2015). First principles phonon calculations in materials science. *Scripta Materialia, **108**, 1-5.*

[45] Ziman, J. M. (2001). Electrons and phonons: the theory of transport phenomena in solids. *Oxford university press.*

[46] Perdew, J. P. and Levy, M. (1983). Physical content of the exact Kohn-Sham orbital energies: band gaps and derivative discontinuities. *Physical Review Letters, **51**, 1884.*

[47] Ambrosch-Draxl, C. and Sofo, J. O. (2006). Linear optical properties of solids within the full-potential linearized augmented planewave method. *Computer physics communications, **175**, 1-14.*

[48] Bechhoefer, J. (2011). Kramers–Kronig, Bode, and the meaning of zero. *American Journal of Physics, **79**, 1053-1059.*

[49] Fox, M. (2010). Optical properties of solids (Vol. 3). *Oxford University Press.*